ELSEVIER

PII: S0266-3538(98)00039-6

Composites Science and Technology **58** (1998) 1741–1751

Printed in Great Britain
0266-3538/98 $—see front matter

THE EFFECT OF RESIDUAL STRESSES AND SAMPLE PREPARATION ON PROGRESSIVE DEBONDING DURING THE FIBER PUSH-OUT TEST

V. T. Bechel[a]* & N. R. Sottos[b]

[a]*Nonmetallic Structural Materials Branch, AFRL/MLBC, Building 654, 2941 P Street Suite 1, Wright Patterson AFB, OH 45433-7750, USA*

[b]*Theoretical and Applied Mechanics Deptartment, University of Illinois at Urbana-Champaign, Champaign, IL, USA*

(Received 22 August 1997; revised 3 November 1997; accepted 6 February 1998)

Abstract

Iterative finite-element analyses have been conducted to determine the debond length as a function of force during progressive debonding in fiber push-out tests. This procedure was applied to data from push-out tests on a steel/epoxy model composite. During push-out testing this composite debonded from the bottom (support) face of the sample. The modeling allowed debonding from the bottom and included pre-existing debonds caused by residual stresses and/or sample preparation. The predicted debond lengths were within 10% of the measured debond lengths. Evidence is also shown that cutting and polishing can cause debonds that are longer than one third of the sample thickness in samples with a relatively small diameter steel fiber. © *1998 Elsevier Science Ltd. All rights reserved*

Keywords: A. polymer-matrix composites, B. debonding, C. fracture, B. friction, C. finite-element analysis

1 INTRODUCTION

The fiber push-out test is one of the most commonly used methods of obtaining interface properties. The test involves pushing a single fiber out of a thin slice of composite while measuring applied force and push-out tool displacement. The force/displacement curve recorded during the push-out experiment is later related to the interface mode II toughness and the coefficient of friction between the fiber and matrix (assuming Coulomb friction) by fitting the data to either an analytical or a finite-element solution.

Approximate theories based on the shear-lag assumption (load transfer by shear from an infinite matrix to a fiber) have been developed to convert the force/displacement data from push-out experiments to interface properties.[1–6] All of these closed-form solutions assume that the debond grows along the interface from the top to the bottom of the sample. In a previous related piece of work, Bechel and Sottos[7] used a method of successive finite-element analyses to predict debond length in a top debonding model composite consisting of polyester fibers in an epoxy matrix. The finite-element calculation of debond length was significantly more accurate than shear-lag predictions in relatively thin samples.

Many composites do not debond from the top during fiber push-out tests. Koss *et al.*[8] and Eldridge[9] discovered that in selected metal-matrix composites the interface initially debonded from the bottom. The location of initial debonding was determined by interrupting the push-out test before the peak load and examining the top and bottom surface. Bechel and Sottos[10] showed that epoxy matrix composites with large residual stresses and/or large fiber to matrix moduli ratio tend to debond from the bottom. Experiments were conducted to measure the debond length in a bottom debonding steel/epoxy model composite. Their experiments consisted of observing the development of photoelastic fringes in the matrix during the progressive debonding phase of fiber push-out tests carried out in a circular polariscope. A concentration of the isochromatic fringes along the interface indicated the location of the debond tip. In the current work the method of successive finite-element analyses used by Bechel and Sottos[7] is applied to predict the debond length for a bottom debonding composite consisting of a steel fiber in an epoxy matrix. A comparison between the finite-element calculated debond length and the photoelastically measured debond length is made.

Several previous investigators have developed computational methods that can be applied to the bottom debonding fiber push-out problem. Kallas *et al.*[11] used the finite-element method to calculate the stress distribution in a fully bonded thin slice fiber push-out sample of sapphire fibers in a niobium matrix under typical pre-debonding loads. Kallas and co-workers

*To whom correspondence should be addressed.

showed that the relative magnitudes of the peak in the shear stress (an artifact of the method's inability to capture the stress singularity) near the top and near the bottom of the interface is affected by the sample thickness and the support hole size relative to the fiber diameter. An interface crack was not included in the model, but their work indicated shear stress due to a large drop in temperature during processing and interfacial tensile radial stress due to bending of thin samples may be the cause of debonding from the bottom during push-out testing.

Chandra and Ananth[12] also used the finite-element method to model debonding during fiber push-out tests. Debond length was predicted by finite-element simulations of the fiber push-out test but was not compared with experimentally measured debond length data. The maximum shear stress, $(\tau_{rz})_{max}$, along the interface calculated with the finite-element method was chosen as the failure criterion. Force/displacement curves were generated by finite-element analyses for several interface strengths and then compared with an experimental force/displacement curve. The interface strength that corresponded to the best curve fit was chosen. This method is potentially powerful because the location of initial debonding and even the possibility of debond growth occurring from both ends of the sample at the same time could be predicted and included in the model. A drawback of Chandra and Ananth's formulation is their use of a maximum shear-stress criterion in the presence of an elastic singularity for characterizing resistance to growth of a sharp crack.

The concentric cylinders variational model developed by Tandon and Pagano[13] was used to study the interaction of an annular matrix crack with an interface crack in a composite. The composite was uniformly strained longitudinally, and the interface consisted of a combination of open, slipping and sticking zones. Discretization was required only in the radial direction with the axial and hoop stresses assumed to vary linearly in the radial direction within each element. This model was employed by Tandon and Pagano[14] to solve fiber push-out problems similar to the problems solved by Bechel and Sottos[7] with the finite-element method. As in the finite-element method, the formulation of Tandon and Pagano[14] included the exact (in the elasticity sense) boundary conditions imposed on the top and bottom of the push-out sample during testing. The debonded part of the interface was allowed to open if a tensile interfacial radial stress developed, and Coulomb friction was incorporated in the slipping zone of the interface. The debond lengths predicted by Tandon and Pagano based on data from fiber push-out tests on a polyester/epoxy model composite were in agreement with the results of Bechel and Sottos.[7] This model could also be used to study a bottom debond.

The present finite-element solution includes residual stresses and determines the debond length as a function of force from experimental load-deflection data, independent of a criterion for interface debonding. Both a top and a bottom debond are included when necessary, and the development of a frictional shear stress on the appropriate debonded portion(s) of the interface is included in the interface boundary conditions.

2 STEEL/EPOXY MODEL COMPOSITE

Single fiber steel/epoxy model composite bars were prepared by placing a 1·65 mm diameter steel fiber in a 50 mm long mold which was then filled with epoxy (EPON 828/PACM). Table 1 lists the properties of the steel fiber and epoxy matrix at room temperature. The model composite was cured at 150°C, resulting in a temperature drop of 125°C. After removal from the mold, debonds 3 mm to 6 mm long on each end of the sample were observed and measured photoelastically.

Two sets of push-out samples were prepared from the composite bars, as schematically shown in Fig. 1. Set I was prepared by cutting samples 12·6 mm long from the center of the 50 mm bars (Fig. 1(a)). Debonds 0·5–1·5 mm long immediately formed at the top and bottom of the interface due to residual stresses. These debonds, designated as l_{i1} and l_{i2} were carefully measured photoelastically and included in the finite-element analysis. Set II was prepared by cutting the samples from the 50 mm bars such that the samples included material adjacent to one of the 3–6 mm long debonds formed on the 50 mm bar as shown in Fig. 1(b). Using a relatively long mold and cutting the samples far from the ends of the 50 long composite bars (as the samples in set I were) was necessary to obtain measured debond lengths which were consistent with the calculated debond lengths. The issue of which portion of the raw composite should be used as the push-out sample is discussed further in Section 4.

The load, displacement and bottom debond length measured by Bechel and Sottos[10] during a displacement controlled push-out test on a steel/epoxy sample from set I is shown in Fig. 2. As a result of the removal of the machine compliance (the deflection of the test fixture), a large discontinuity in load and displacement at total debond is apparent in the load/displacement curve (represented with a dashed line). Both a top and a bottom debond, each 0·5 mm long, were measured photoelastically in this sample after cutting it from the 50 mm long composite bar. Since the length of the top debond remained constant throughout the push-out test, its length was not plotted in Fig. 2. The length of the bottom debond was intentionally increased from 0·5 mm to

Table 1. Properties of fiber and matrix in model composite

Property	Fiber	Matrix
Young's modulus	200 GPa	2.5 GPa
Poisson's ratio	0·30	0·35
Coefficient of thermal expansion	12×10^{-6}/°C	68×10^{-6}/°C

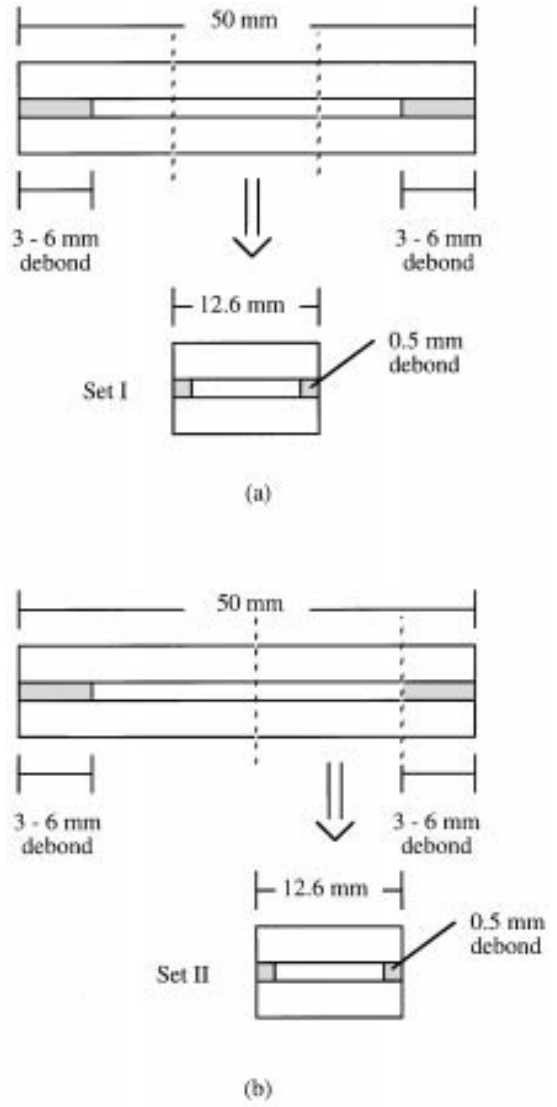

Fig. 1. Sample preparation: (a) set I was cut from the center of the raw composite bars; (b) set II was cut to include material near the debonds in the raw composite bars.

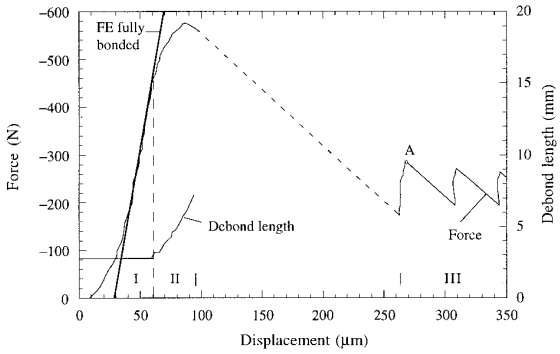

Fig. 2. Force and debond length versus displacement curves from a steel/epoxy push-out test. $r_f = 0{\cdot}825$ mm, $t = 12{\cdot}60$ mm, $r_s = 1{\cdot}025$ mm, $r_o = 3{\cdot}74$ mm, and $r_p = 0{\cdot}70$ mm.

2·8 mm by applying a load to the top of the fiber prior to the push-out test. As shown in Fig. 2, during the push-out test the bottom debond length remained at 2·8 mm as the load increased from 0 N to −460 N. The bottom debond then grew toward the top of the sample until it reached the 0·5 mm top debond at the peak load. This pattern of interface failure was consistent in all of the steel/epoxy samples.

The coefficient of friction was obtained by applying the shear-lag theory of Kerans and Parthasarathy.[5] The use of the frictional data to compute μ was somewhat ambiguous because the portion of the push-out curve after total debond was composed of alternating regions of stick and slip. The entire fiber slipped approximately 170 μm immediately after total debond. Following the load drop at total debond the punch load again built up without further slip until the first peak was reached. Since additional slippage would not occur at loads lower than the first peak load in the frictional data, this value (shown as point A in Fig. 2) is thought to be the most appropriate load for calculating μ rather than the average between the first peak and the first trough.

The equation

$$l_e = \frac{r_f}{2\mu k}\ln\left(\frac{P^* - F}{P^*}\right) \tag{1}$$

from Kerans and Parthasarathy[5] relating embedded length, l_e, to applied load, F, during frictional push-out was used to calculate μ for an embedded length of 12·37 mm and an applied load of −283 N. In eqn (1) r_f is the radius of the fiber, k is a constant that depends on the elastic properties of the fiber and matrix, and P^* is directly related to the average residual radial stress at the interface. The solution of eqn (1) results in a coefficient of friction of 0·33. A full discussion of the accuracy of shear-lag theory when computing the coefficient of friction from the frictional portion of push-out data is given in Bechel and Sottos.[7] This result for the coefficient of friction is consistent with the range of $\mu = 0{\cdot}37$–$0{\cdot}44$ reported by Yamaguchi[15] for a steel/epoxy interface. Yamaguchi determined the coefficient of friction by measuring the angle of incline necessary to initiate sliding of a planar sample (treated as a rigid body) on an inclined plane.

3 CALCULATION OF DEBOND LENGTH

3.1 Finite-element model

The geometry of the fiber push-out problem is shown in Fig. 3. An axisymmetric model is assumed with r as the radial coordinate originating at the fiber central axis and z as the axial coordinate originating at the bottom of the sample. The radii of the punch, fiber, support and outer edge of the matrix are r_p, r_f, r_s and r_o, respectively. One or more portions of the fiber may be debonded.

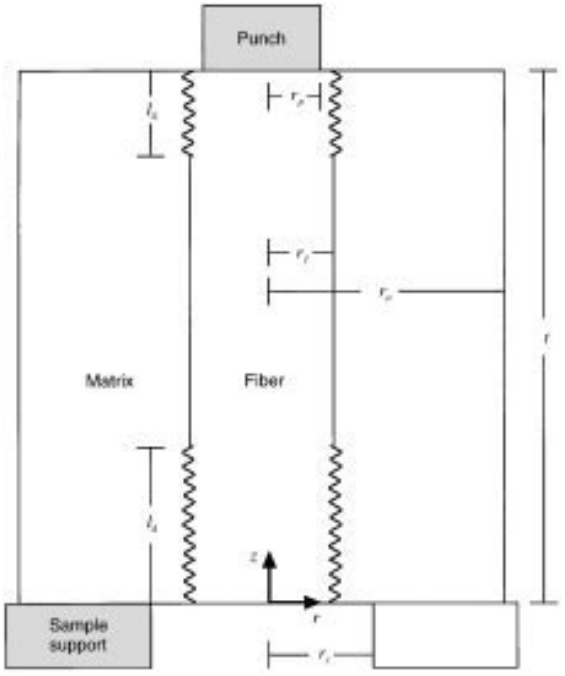

Fig. 3. Schematic of the coordinate axes and relevant dimensions for the push-out problem.

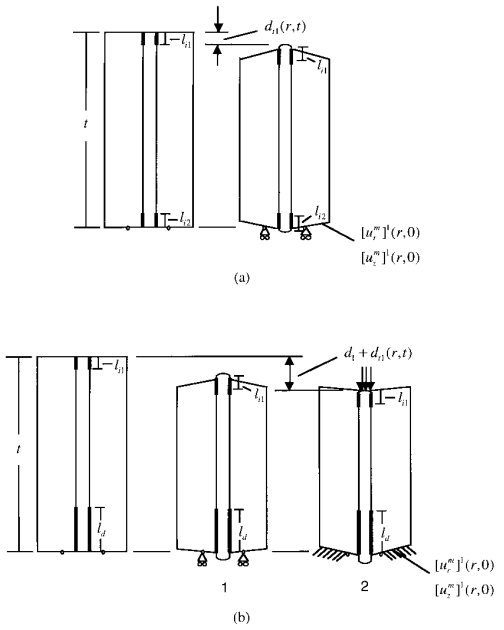

Fig. 4. Schematic of finite-element analysis boundary conditions for steel/epoxy: (a) for the first finite-element run, only the initial debonds are present; (b) for the second finite-element run, the bottom debond is lengthened.

Two debonds are included in Fig. 3. The bottom debond caused by the punch load plus residual stresses has length l_d, and l_{i1} is the length of the top debond resulting from residual stresses. The sample thickness in the axial direction is denoted by t. A discussion of the finite-element solution is given in Appendix A, since the details are the same as in Bechel and Sottos.[7]

3.2 Modeling procedure

The two steps in the finite-element simulation are illustrated in Fig. 4. The relevant displacements at the top of the fiber are compared schematically in Fig. 5. The thermal load in Fig. 4(a) and step 1 of Fig. 4(b) is caused by the differential shrinkage between the fiber and the matrix during processing. The stress due to chemical shrinkage is assumed to be much smaller than the stress due to the difference in coefficients of thermal expansion, because the chemical reaction is nearly completed at the peak processing temperature when the matrix is above its glass transition temperature and can sustain very little stress.

The displacement function $d_{t1}(r,t)$ is the thermal displacement of the top of the fiber when only the initial debonds due to processing are present, and $d_{t2}(r,t)$ is the thermal displacement of the fiber when the top initial debond is present and the bottom debond is lengthened to l_d by the push-out load. For this bottom debonding system $|d_{t1}(r,t)| < |d_{t2}(r,t)|$. The bottom debond caused by the push-out load (length l_d) is longer than the initial debond (length l_{i2}) so the debond of length l_d allows the top of the fiber to move downward more under the thermal load from processing. Because the bottom debond grows to length l_d only after the punch has displaced the fiber, $d_{t1}(r,t)$ is used as the reference displacement of the fiber top surface after processing.

A simulation of the initial linear part of the force/displacement curve was conducted by applying increasing loads in step 2 of Fig. 4(b) without increasing the debond length ($l_d = l_{i2}$) because the bottom debond had not grown past its initial length for that part of the push-out data. The slope of the data ($15{\cdot}5\,\mathrm{N}\,\mu\mathrm{m}^{-1}$) in section I of Fig. 2 (loading before progressive debonding) was predicted with less than a 1% error by the finite-element solution. This comparison in the linear region verifies the choice of $d_{t1}(r,t)$ rather than $d_{t2}(r,t)$.

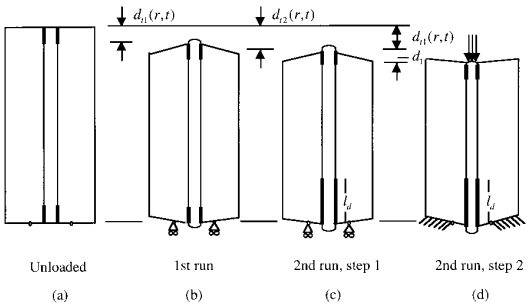

Fig. 5. Relative displacement at the top of the fiber for each phase of the steel/epoxy finite-element analysis: (a) unloaded; (b) actual deformation from thermal shrinkage; (c) thermal shrinkage with bottom debond lengthened; (d) displacement from push-out test added.

The procedure for deriving force versus debond length from force and displacement pairs chosen from the progressive debonding portion of the steel/epoxy push-out data was the same as for polyester/epoxy.[7] A load/displacement pair, (d_1,F_1) was chosen from progressive debonding. An arbitrary value for l_d was initially used in the finite-element mesh along with the chosen displacement. If the resulting load did not correspond to the chosen load, F_1, the debond length was adjusted and a solution was obtained for the same punch displacement, d_1, and the new debond length. The debond length, which could consist of slip and/or open regions, was adjusted until the chosen load/displacement pair was regenerated by the finite-element simulation.

The boundary and continuity conditions for the calculation of $d_{t1}(r, t)$ and the radial and axial displacements of the bottom nodes are shown schematically in Fig. 4(a) and listed in Table 2. The boundary and continuity conditions for the application of the thermal load from processing and the punch load from push-out testing are shown schematically in Fig. 4(b) and listed in Tables 3 and 4. In addition to the listed boundary conditions, it is further required that the interfacial shear stress along any of the closed and slipping portions of the interface must oppose the relative slip.

3.3 Results

The debond length versus force computed with the finite-element analysis from the compliance of the force/displacement curve in Fig. 2 is compared with the measured debond length in Fig. 6. The finite-element predicted debond length remains within 5% of the measured debond length for the first 1·5 mm of debond growth and within 10% of the measured debond length for the final 1·7 mm of debond growth. The increasing error for larger debond length may be caused by an underestimate of the coefficient of friction. The portion of the axial load generated by friction becomes more significant as the debond length increases. Therefore, an accurate coefficient of friction is more important at longer debond lengths. The data from push-out tests on several samples were analyzed with similar results for μ and the predicted versus measured debond length.

Table 2. Boundary and continuity conditions for differential shrinkage during cooldown after processing for the mesh with initial top debond of length l_{i1} and bottom debond of length l_{i2} (schematically shown in Fig. 4(a))

$z=0$	$\sigma^{f}_{rz}(r,0)=\sigma^{f}_{zz}(r,0)=0$	$0\le r\le r_f$
	$\sigma^{m}_{rz}(r,0)=\sigma^{m}_{zz}(r,0)=0$	$r_f\le r\le r_o$
	$u^{m}_{z}(r_s,0)=0$	
$z=t$	$\sigma^{f}_{rz}(r,t)=\sigma^{f}_{zz}(r,t)=0$	$0\le r\le r_f$
	$\sigma^{m}_{rz}(r,t)=\sigma^{m}_{zz}(r,t)=0$	$r_f\le r\le r_o$
$r=0$	$u^{f}_{r}(0,z)=0$	$0\le z\le t$
$r=r_f$	$\sigma^{f}_{rr}(r_f,z)=\sigma^{m}_{rr}(r_f,z)$	$0\le z\le t$
	$\sigma^{f}_{rz}(r_f,z)=\sigma^{m}_{rz}(r_f,z)$	$0\le z\le t$
	$u^{f}_{r}(r_f,z)=u^{m}_{r}(r_f,z)$	$l_{i2}\le z\le t-l_{i1}$
	$u^{f}_{z}(r_f,z)=u^{m}_{z}(r_f,z)$	$l_{i2}\le z\le t-l_{i1}$
	$\sigma^{f}_{rr}(r_f,z)=\sigma^{m}_{rr}(r_f,z)\le 0$	$0\le z\le l_{i2}$ and $t-l_{i1}\le z\le t$
	$\lvert\sigma^{f}_{rz}(r_f,z)\rvert=\lvert\sigma^{m}_{rz}(r_f,z)\rvert\le\lvert\mu\sigma^{f}_{rr}(r_f,z)\rvert=\lvert\mu\sigma^{m}_{rr}(r_f,z)\rvert$	$0\le z\le l_{i2}$ and $t-l_{i1}\le z\le t$
	$u^{f}_{r}(r_f,z)=u^{m}_{r}(r_f,z)$ for $\sigma^{f}_{rr}(r_f,z)=\sigma^{m}_{rr}(r_f,z)<0$	$0\le z\le l_{i2}$ and $t-l_{i1}\le z\le t$
	$u^{f}_{r}(r_f,z)\le u^{m}_{r}(r_f,z)$ for $\sigma^{f}_{rr}(r_f,z)=\sigma^{m}_{rr}(r_f,z)=0$	$0\le z\le l_{i2}$ and $t-l_{i1}\le z\le t$
$r=r_o$	$\sigma^{m}_{rr}(r_o,z)=\sigma^{m}_{rz}(r_o,z)=0$	$0\le z\le t$

Table 3. Boundary and continuity conditions for differential shrinkage during cooldown after processing for the mesh with initial top debond of length l_{i1} and bottom debond length of l_d (schematically shown in Fig. 4(b), step 1)

$z=0$	$\sigma^{f}_{rz}(r,0)=\sigma^{f}_{zz}(r,0)=0$	$0\le r\le r_f$
	$\sigma^{m}_{rz}(r,0)=\sigma^{m}_{zz}(r,0)=0$	$r_f\le r\le r_o$
	$u^{m}_{z}(r_s,0)=0$	
$z=t$	$\sigma^{f}_{rz}(r,t)=\sigma^{f}_{zz}(r,t)=0$	$0\le r\le r_f$
	$\sigma^{m}_{rz}(r,t)=\sigma^{m}_{zz}(r,t)=0$	$r_f\le r\le r_o$
$r=0$	$u^{f}_{r}(0,z)=0$	$0\le z\le t$
$r=r_f$	$\sigma^{f}_{rr}(r_f,z)=\sigma^{m}_{rr}(r_f,z)$	$0\le z\le t$
	$\sigma^{f}_{rz}(r_f,z)=\sigma^{m}_{rz}(r_f,z)$	$0\le z\le t$
	$u^{f}_{r}(r_f,z)=u^{m}_{r}(r_f,z)$	$l_d\le z\le t-l_{i1}$
	$u^{f}_{z}(r_f,z)=u^{m}_{z}(r_f,z)$	$l_d\le z\le t-l_{i1}$
	$\sigma^{f}_{rr}(r_f,z)=\sigma^{m}_{rr}(r_f,z)\le 0$	$0\le z\le l_d$ and $t-l_{i1}\le z\le t$
	$\lvert\sigma^{f}_{rz}(r_f,z)\rvert=\lvert\sigma^{m}_{rz}(r_f,z)\rvert\le\lvert\mu\sigma^{f}_{rr}(r_f,z)\rvert=\lvert\mu\sigma^{m}_{rr}(r_f,z)\rvert$	$0\le z\le l_d$ and $t-l_{i1}\le z\le t$
	$u^{f}_{r}(r_f,z)=u^{m}_{r}(r_f,z)$ for $\sigma^{f}_{rr}(r_f,z)=\sigma^{m}_{rr}(r_f,z)<0$	$0\le z\le l_d$ and $t-l_{i1}\le z\le t$
	$u^{f}_{r}(r_f,z)\le u^{m}_{r}(r_f,z)$ for $\sigma^{f}_{rr}(r_f,z)=\sigma^{m}_{rr}(r_f,z)=0$	$0\le z\le l_d$ and $t-l_{i1}\le z\le t$
$r=r_o$	$\sigma^{m}_{rr}(r_o,z)=\sigma^{m}_{rz}(r_o,z)=0$	$0\le z\le t$

4 IMPORTANCE OF SAMPLE PREPARATION

4.1 Interface slippage during processing

The set II samples were studied next. These samples were obtained by removing the 3–6 mm debonds from the composite bars and cutting the samples from one end of each of the shortened composite bars (Fig. 1(b)). When the set II samples were push-out tested and modeled, the bottom debond length was severely underpredicted. The debond lengths calculated were, in general, only 20% of the measured lengths. The underpredicted debond lengths can be explained with the following hypothesis (presented in Fig. 7(a)–(e)) about the events during the cooldown phase of processing for steel/epoxy.

Figure 7(a) shows a schematic of a steel fiber embedded in an epoxy matrix at the peak processing temperature of 150°C. The sample is stress free. As the temperature drops below the processing temperature to T_1, a large τ_{rz} shear stress and a tensile radial stress

Table 4. Boundary and continuity conditions for fiber pushout of the mesh with initial top debond of length l_{i1} and bottom debond length of l_d(schematically shown in Fig. 4(b), step 2)

$z=0$	$\sigma^{f}_{rz}(r,0)=\sigma^{f}_{zz}(r,0)=0$	$0\le r\le r_f$
	$\sigma^{m}_{rz}(r,0)=\sigma^{m}_{zz}(r,0)=0$	$r_f\le r\le r_s$
	$u^{m}_{r}(r,0)=[u^{m}_{r}]^{1}(r,0)$	$r_s\le r\le r_o$
	$u^{m}_{z}(r,0)=[u^{m}_{z}]^{1}(r,0)$	$r_s\le r\le r_o$
$z=t$	$u^{f}_{z}(r,t)=d_{t1}(r,t)+d_1$	$0\le r\le r_p$
	$\sigma^{f}_{rz}(r,t)=0$	$0\le r\le r_f$
	$\sigma^{f}_{zz}(r,t)=0$	$r_p\le r\le r_f$
	$\sigma^{m}_{rz}(r,t)=\sigma^{m}_{zz}(r,t)=0$	$r_f\le r\le r_o$
$r=0$	$u^{f}_{r}(0,z)=0$	$0\le z\le t$
$r=r_f$	$\sigma^{f}_{rr}(r_f,z)=\sigma^{m}_{rr}(r_f,z)$	$0\le z\le t$
	$\sigma^{f}_{rz}(r_f,z)=\sigma^{m}_{rz}(r_f,z)$	$0\le z\le t$
	$u^{f}_{r}(r_f,z)=u^{m}_{r}(r_f,z)$	$l_d\le z\le t-l_{i1}$
	$u^{f}_{z}(r_f,z)=u^{m}_{z}(r_f,z)$	$l_d\le z\le t-l_{i1}$
	$\sigma^{f}_{rr}(r_f,z)=\sigma^{m}_{rr}(r_f,z)\le 0$	$0\le z\le l_d$ and $t-l_{i1}\le z\le t$
	$\lvert\sigma^{f}_{rz}(r_f,z)\rvert=\lvert\sigma^{m}_{rz}(r_f,z)\rvert\le\lvert\mu\sigma^{f}_{rr}$	$0\le z\le l_d$ and $t-l_{i1}\le z\le t$
	$(r_f,z)\rvert=\lvert\mu\sigma^{m}_{rr}(r_f,z)\rvert$	
	$u^{f}_{r}(r_f,z)=u^{m}_{r}(r_f,z)$ for $\sigma^{f}_{rr}(r_f,z)$	$0\le z\le l_d$ and $t-l_{i1}\le z\le t$
	$=\sigma^{m}_{rr}(r_f,z)<0$	
	$u^{f}_{r}(r_f,z)\le u^{m}_{r}(r_f,z)$ for $\sigma^{f}_{rr}(r_f,z)$	$0\le z\le l_d$ and $t-l_{i1}\le z\le t$
	$=\sigma^{m}_{rr}(r_f,z)=0$	
$r=r_o$	$\sigma^{m}_{rr}(r_o,z)=\sigma^{m}_{rz}(r_o,z)=0$	$0\le z\le t$

develop along the interface near the fiber ends (Fig. 7(b)). If the fiber-matrix bond is not strong enough, the interface may open due to the tensile radial stress or remain closed and slip due to the shear stress. Debonds will form at the fiber ends as shown in Fig. 7(c). As discussed earlier, these debonds were observed in the steel/epoxy samples (3–6 mm long after cooldown). The debonds form near the fiber ends partly because the bond between steel and epoxy is relatively weak, and partly because the radial stress (zero in the open zone if an open zone develops) is relatively small or tensile at T_1. The debonds grow to a length that allows the friction along the closed portion of the debonded ends to relieve some of the interfacial shear

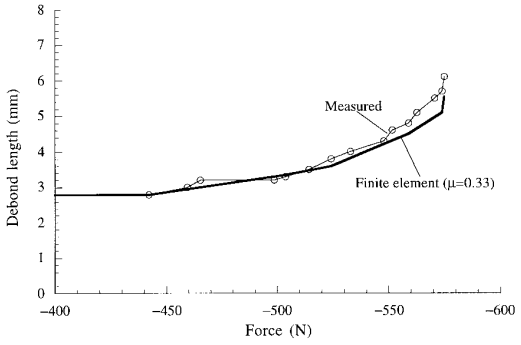

Fig. 6. A comparison of the measured and finite-element predicted debond lengths for the push-out curve shown in Fig. 2.

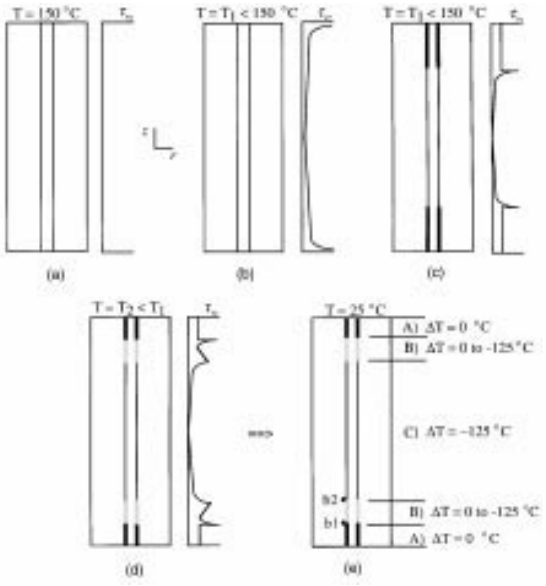

Fig. 7. Schematic of interface bonding for steel/epoxy as cooldown progresses during processing.

stress which develops at the debond tips from differential shrinkage in the axial direction.

Figure 7(d) shows the sample after further cooling. The compressive radial stress increases, forcing the matrix into better contact with the fiber surface and possibly closing some of the open zone (if an open zone had previously developed). The closed portion of the interface can sustain a larger shear stress and is more resistant to slipping. It is postulated that a portion of each of the debonds, toward the middle cross-section, stops slipping and sticks to the fiber as the temperature drops further. The total length of the slip zone plus the open zone decreases continuously during cooldown until room temperature is reached.

If this mechanism actually occurs during cooldown, at room temperature the interface would be divided into three sections as shown in Fig. 7(e). Section A is the debonded portion at each end that can be identified by viewing the photoelastic fringes after cooldown. As Fig. 1 shows, the samples were cut from the composite bars such that these debonded portions were not a part of either set of samples. Section B contains the portions of the interface that debonded at a relatively high temperature and later stopped slipping at some temperature between 150°C and room temperature. The magnitude of the axial residual stress induced on either side of the interface in this section does not correspond to a ΔT of −125°C, as was assumed by the finite-element simulation of fiber push-out. The magnitude of axial residual stress in the fiber varies from a minimum at the limit of section B toward the fiber end (b1) to a maximum at the limit of section B toward the fiber middle cross-section (b2). In section C, the interface did not debond during the entire cooldown.

Assuming this cooldown hypothesis is correct, the samples in set I would contain only a section C, since they were cut far from the ends of the raw composite, and the samples in set II would contain a section B at one end of the sample and section C over the remainder of the sample. The difference between the actual residual stresses in section B and the residual stresses calculated, based on assuming a perfect bond in section B throughout cooldown, may be the source of the error in predicting debond length for the set II samples.

4.2 Fiber extension tests

An experiment was conducted to study the cooldown hypothesis. Three steel/epoxy push-out samples were prepared by the same steps as the set II samples. A schematic of one of these samples is shown in Fig. 8(a). Since the ends were debonded, the fiber ends extended a short distance beyond the matrix (approximately 5 μm). The push-out fixture used for the fiber push-out tests was capable of measuring the length of exposed fiber, and is shown schematically in Fig. B1. The push-out fixture is described in Appendix B since it was identical to the set-up used by Bechel and Sottos.[10]

A sample was placed on the sample support, and the punch was lowered until it was near the fiber surface but not in contact with the surface as evidenced by a zero load on the load cell. The punch was lowered further until a load ($<0{\cdot}2$ N) registered on the load cell. This location was used as a reference height. The punch was moved laterally until it was entirely over the matrix, and then it was lowered to the matrix surface. This routine was repeated at four locations 90° apart on the matrix within 20 μm of the fiber lateral surface to measure the difference in height between the matrix and the reference location (bottom of the fiber). The four measurements were averaged and recorded as the length of exposed fiber to within ± 1 μm. This first measurement of exposed fiber length was used as a reference length and not compared to the finite-element prediction of exposed fiber length because the process of cutting off the ends of the sample may have removed some of the exposed fiber end.

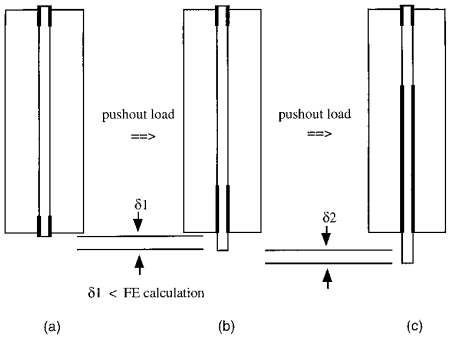

Fig. 8. The fiber extension measurement: (a) schematic of unloaded sample; (b)(c) schematic of two samples with longer bottom debond lengths.

After the initial measurement of exposed fiber was conducted, the sample was turned over so the measured end was over the sample support hole, and a compressive load was applied to the top of the fiber until the bottom debond grew to 3 mm as schematically shown in Fig. 8(b). This debond grew from its original length (0·5–1·5 mm) to a length of 3 mm through part or all of the section B region. The debond length was once again measured by observing the density of photoelastic fringes produced by a circular polariscope as described by Bechel and Sottos.[10] A description of the equipment used for the debond length measurement is given in Appendix B.

The composite sample was turned over again so that the end with the 3 mm debond was upward. The exposed length, δ_1, was measured. δ_1 is the increase in exposed fiber length due to the additional debond growth. Finite-element analyses on both a model of the sample with the interface conditions shown in Fig. 8(a) and another with the interface conditions shown in Fig. 8(b) were conducted. A thermal load of -125°C was applied in each case. The boundary and continuity conditions for the finite-element analyses were the same as schematically shown in Fig. 4(b), step 1. A coefficient of friction of $\mu = 0{\cdot}33$ was used. The difference in the exposed fiber length at the bottom was extracted from the finite-element analysis and found to be, on average, about 30% more than the measured difference, δ_1.

Similarly, the debond was grown to 6 mm and the additional exposed fiber length, δ_2, was measured. The measured δ_2, on average, was within 5% of the finite-element predicted δ_2. A total of three samples were tested with similar results. These measurements and finite-element simulations revealed that the amount of residual axial stress released by debond growth was less than expected in the early stages of debonding and closer to the expected amount as the interface crack grew further from the sample surface. The difference between the measured and the calculated change in exposed fiber length could be the result of less residual axial stress near the ends of the sample than would develop from $\Delta T = -125$°C. These results are consistent with the present hypothesis about the cooldown phase of processing for the steel/epoxy model composite.

4.3 Inconsistent push-out curves

The theory about cooldown also explains a commonly observed phenomenon, depicted in Fig. 9, that was observed in the steel/epoxy push-out data from some of the set II samples. A line through and extending from the initial linear part of the force/displacement curve is provided to indicate where the sample becomes more compliant from debond growth. An increase in debond length of 1·2 mm beyond the initial debond length occurs without any noticeable non-linearity in the force versus displacement curve. The release of axial residual stress in the debonded portion of the fiber and the relaxation in the axial direction of the matrix around

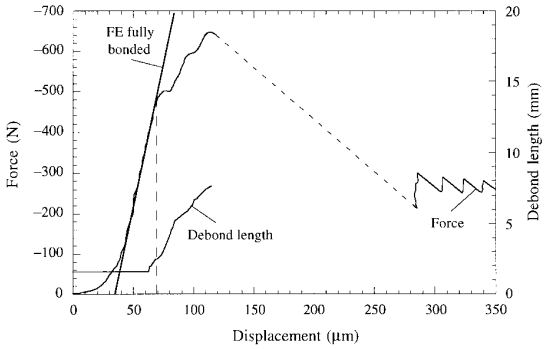

Fig. 9. Push-out curve from a steel/epoxy sample cut from section B and C. Debond length increases 1·2 mm before the force/displacement curve becomes non-linear.

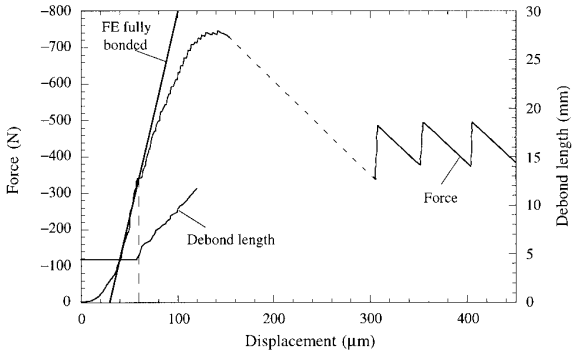

Fig. 10. Push-out curve from a steel/epoxy sample cut from section B and C. After initial non-linearity, the slope of the force/displacement curve remains constant over a significant additional displacement.

the debonded portion of the fiber contribute to the departure of the force/displacement curve from linearity. If there was very little release of residual stress in the initial stages of debonding, there would be less tendency of the force/displacement curve to turn over when debond growth begins.

A similar but slightly different phenomenon, shown in Fig. 10, also occurred in the push-out curves from some of the set II specimens. The debond growth begins almost at the instant the force/displacement curve separates from the line drawn through the pre-progressive debonding portion of the data. The inconsistency happens between −350 N and −475 N. The force/displacement curve has approximately the same slope as the line through the initial linear part of the push-out data even though the debond length grows more than 2 mm during this period. The sample should become more compliant as residual stress is unloaded from the bottom end of the fiber during debonding, allowing the top face of the fiber to move downward, but the sample compliance remains nearly constant. A smaller than expected (possibly near zero) axial residual stress in several millimeters of the fiber near the ends of the sample would also help explain this result.

The image in Fig. 11(a) shows the photoelastic fringe pattern from an uncut single fiber steel/epoxy composite bar after cooldown. The fringes near the fiber ends are related to the magnitude of residual shear stress in the epoxy while the shear stress must be near zero away from the fiber ends since no fringes are apparent at points over 10 mm from the ends. A push-out sample cut from the zero shear stress region of the raw material in Fig. 11(a) is shown at the same magnification in Fig. 11(b). The appearance of several photoelastic fringes illustrates the redistribution of stresses, and the points of greatest fringe density near each end of the interface are the tips of new debonds that formed after cutting.

Viscoelastic stress relaxation of the matrix was not suggested as the source of the lower than expected residual axial stresses at the fiber ends because stress relaxation is not consistent with the observation of debonds reforming upon removal of the ends of the composite bars. After processing, debonds were present at the fiber ends as shown in Fig. 1. The debonds were removed and new debonds grew to relieve stress at the fiber ends. If stress relaxation was significant, the removal of the debonds after processing would result in stress relaxation near the ends of the shortened samples—not additional debonding. The cooldown hypothesis of Fig. 7 is consistent with all observed phenomena.

5 INTERFACE FAILURE DUE TO CUTTING

Another factor complicating the analysis of fiber push-out data was observed in scaled-down steel/epoxy push-out samples. Steel fibers, 0·20 mm in diameter (instead of 1·65 mm) were used in these samples, and they were prepared by the same steps as set I of the larger fiber

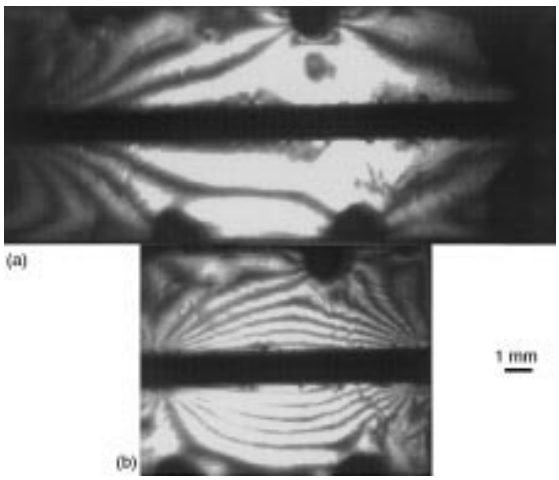

Fig. 11. Photoelastic fringes: (a) due to residual stresses in a long steel/epoxy bar; (b) due to residual stresses in a sample cut from the center of (a).

diameter samples. The normalized sample thickness of approximately 12 fiber diameters was the same as in the 1·65 mm fiber diameter samples.

Prior to push-out testing, two distinct fringes were observed on either side of the fiber along the middle one third of the fiber, where the fiber was still bonded to the matrix. For the larger fiber diameter of 1·65 mm, initial debonds with an absolute length of 0·5–1·5 mm were measured, and for the same composite with the smaller fiber diameter, the initial debonds were 0·5–0·8 mm. Therefore, the initial debonds in the small fiber diameter samples were much longer in terms of normalized length—2·5–4·0 fiber diameters for the small fiber compared with 0·3–0·9 fiber diameters for the large fiber). If the initial debonds grew owing to residual stress, their lengths should scale with the fiber diameter—assuming equal interface strengths. The similar range of absolute lengths of the initial debonds indicates that the initial debonds may have been produced by the combination of residual stresses and another mechanism such as cutting. Interface debonding that occurred as a result of cutting may have been more significant in the 0·20 fiber diameter samples. Cutting of the specimens was accomplished with a flat-faced diamond wafering blade which created a path through the composite by wearing away the material in front of the blade face. As the blade approached the interface, the process of grabbing and tearing material in its path most likely exerted a tensile normal stress and/or $\tau_{r\theta}$ shear stress on a portion of the interface near and including the interface in the path of the blade. These stresses would contribute to debonding near the ends of the samples.

The top and bottom faces of the push-out samples were polished to a 15 μm finish to determine whether polishing would cause further fiber debonding. No change in the photoelastic fringe patterns could be detected after polishing. A push-out test was then carried out on each sample. After the push-out test, the original fringes that were parallel to the fiber were no longer observed, verifying that the presence of fringes indicates the presence of interface adhesion. The applied axial stress necessary to debond the 0·20 mm diameter steel fiber was 50% greater than the axial stress required to totally debond the larger fiber diameter samples. This result indicates that the scaled-down steel/epoxy samples had a greater interface strength than the 1·65 mm fiber diameter samples. An interface with a greater strength would be more resistant to debonding. Therefore, the larger normalized length of the initial debonds in the small diameter samples was not a result of the interface strength in the small diameter samples being less that the interface strength in the large diameter samples. These experiments show that as the fiber diameter and absolute sample thickness are reduced, the likelihood of the samples containing initial debonds that extend over a large portion of the sample thickness increases.

6 DISCUSSION AND CONCLUSIONS

The finite-element method was used to analyze push-out data from a bottom debonding composite with residual stresses large enough to debond the fiber ends during processing. The position within the raw composite that the test specimen was cut from was shown to be critical to the calculation of debond length for this steel/epoxy system. When data were analyzed from samples cut near the ends of the raw composite (set II), the debond length was grossly underestimated. The force/displacement curves from these samples often showed no decrease in stiffness during the initial stages of debond growth. Force versus displacement data from test samples cut at least 6 fiber diameters from the ends of the raw composite (set I) became non-linear at the onset of debond growth, as intuitively expected, with the slope continuously decreasing as a function of debond growth. Application of the iterative finite-element method used in Bechel and Sottos[7] to the data from the set-I samples yielded calculated debond lengths within 10% of the measured debond lengths.

A theory was proposed to explain why the proximity of the test sample to the ends of the raw composite affected the push-out results. It was hypothesized that a portion of the interface opened and/or slipped during the first stages of cooldown. Part of this debonded portion closed and/or stopped slipping due to increasing radial compressive stress as cooldown progressed. This process resulted in composite bars with three distinct sections—a section that debonded and slipped/opened throughout cooldown, a section that stuck throughout cooldown resulting in a residual stress field corresponding to the entire temperature drop (−125°C), and a section that slipped during a portion of the temperature drop, resulting in a residual stress field corresponding to a temperature drop of less than −125°C. Measurements of the exposed fiber length versus debond length indicated that a smaller residual axial stress was acting near the ends of the fiber in samples cut close to the ends of the raw sample than was calculated with a finite-element analysis.

Although the method described here has been demonstrated to accurately calculate debond length for both a top[7] and a bottom debonding system (even one with debonds present before push-out testing), the level of knowledge required about the condition of the interface and the residual stress state after processing is significant. In general, composite matrices are not transparent and birefringent so the initial debonds, if present, could not be measured in a polariscope prior to push-out testing. Care in sample preparation must be taken to minimize initial debonds in the particular composite that is being tested. In some cases, such as steel/epoxy, debonds from processing and cutting are impossible to avoid completely. If possible, tests should also be done to determine how far the test samples should be cut from the ends of a raw material. The difference in

interface strength calculated from different micromechanical interface strength tests on identical composites,[16] often thought to be attributable to the assumptions made in the analyses, may be partly attributable to the difference in the way in which the samples were prepared and where in the composite the samples were cut from by the different researchers.

One solution to the problem of the inability to measure the length of initial debonds may be to compare the slope of section I of the push-out curve to the finite-element predicted slope. If the finite-element calculation of the slope of the initial linear part of the curve is too stiff, then it could be assumed that initial debonds of equal length at the top and bottom of the fiber are responsible for the difference in stiffness. The equal-length initial debonds could be incorporated in the model and their length adjusted until the finite-element computed slope and the measured slope match. Confidence in the measurement of machine compliance would be necessary for this method to calculate accurately the initial debond length. Also, this method of calculating the initial debond length when it is not possible to measure it assumes that the samples are prepared like the set I samples, i.e. a section B is not present in the samples.

The presence of initial debonds extending up to 4 fiber diameters from the fiber ends was observed in the steel/epoxy model composites with smaller diameter fibers. The normalized length of these initial debonds was 4 times greater than in the larger fiber diameter samples. The greater normalized debond length is evidence that, in addition to the mechanism of relieving residual stress by debonding, another mechanism such as interface damage due to cutting may be a significant cause of initial debonds in smaller diameter samples.

ACKNOWLEDGEMENTS

The authors would like to acknowledge the financial support of the ONR (contract monitor R. Barsoum) and the US Air Force (Senior Knight program). Also, we would like to thank Pranav Shrotriya from the University of Illinois for carrying out the coefficient of thermal expansion measurements.

REFERENCES

1. Gao, Y. C., Mai, Y.-W. and Cotterell, B., Fracture of fiber reinforced materials. *J. Appl. Math Phys.*, 1988, **39**, 550–572.
2. Marshall, D. B. and Oliver, W. C., An indentation method for measuring residual stresses in fiber-reinforced ceramics. *Mater. Sci. Eng.*, 1990, **A126**, 95–103.
3. Hsueh, C. H., Interfacial debonding and fiber pull-out stress of fiber-reinforced composites. *Mater. Sci. Eng.*, 1990, **A123**, 1–11.
4. Liang, C. and Hutchinson, J. W., Mechanics of the fiber push-out test. *Mech. Mater.*, 1993, **14**, 207–221.
5. Kerans, R. J. and Parthasarathy, T. A., Theoretical analysis of the fiber pullout and push-out tests. *J. Am. Ceram. Soc.*, 1991, **74**, 1585–1596.
6. Parthasarathy, T. A., Marshall, D. B. and Kerans, R. J., Analysis of the effect of interfacial roughness on fiber debonding and sliding in brittle matrix composites. *Acta metall. mater.*, 1994, **42**, 3773–3784.
7. Bechel, V. T. and Sottos, N. R., A comparison of calculated and measured debond lengths from fiber push-out tests. *Compos. Sci. Technol.*, 1998, **58**, 1727–1739.
8. Koss, D. A., Hellmann, J. R. and Kallas, M. N., Fiber push-out and interfacial shear in metal matrix composites. *JOM*, 1993, **45**, 34–37.
9. Eldridge, J. I., Elevated temperature fiber push-out testing. *Mater. Res. Soc. Symp. Proc.*, 1995, **365**, 283–290.
10. Bechel, V. T. and Sottos, N. R., Application of debond length measurements to examine the mechanics of fiber pushout. *J. Mech. Phys. Solids*, 1998, **46**, 1675–1697.
11. Kallas, M. N., Koss, D. A., Hahn, H. T. and Hellmann, J. R., Interfacial stress state present in a 'thin-slice' fibre push-out test. *J. Mater. Sci.*, 1992, **27**, 3821–3826.
12. Chandra, N. and Ananth, C. R., Analysis of interfacial behavior in MMCs and IMCs by the use of thin-slice push-out tests. *Compos. Sci. Technol.*, 1995, **54**, 87–100.
13. Tandon, G. P. and Pagano, N. J., Matrix crack impinging on a frictional interface in unidirectional brittle matrix composites. *Int. J. Sol. Struct.*, 1996, **33**, 4309–4326.
14. Tandon, G. P. and Pagano, N. J., Micromechanical analysis of unidirectional composites with frictional interfaces. Paper presented at the ASME Summer Mechanics and Materials, McNU '97, Conference, Northwestern University, Evanston, IL, 1997.
15. Yamaguchi, Y., *Tribology of Plastic Materials*. Elsevier, New York, 1990.
16. Herrara-Franco, P. J. and Drzal, L. T., Comparison of methods for the measurement of fibre/matrix adhesion in composites. *Composites*, 1999, **23**, 2–27.
17. Hibbitt, Karlsson and Sorenson, Inc., *ABAQUS theory manual*. Hibbitt, Karlsson, and Sorenson, Inc., 1994, pp. 5·1·1–5·1·3.

APPENDIX A FINITE-ELEMENT METHOD

The commercial finite-element code ABAQUS (Hibbitt, Karlsson, and Sorenson, Inc.) was used for the finite-element modeling described in this paper. The fiber push-out sample was modeled with second-order axisymmetric isoparametric (CAX8) elements and second-order axisymmetric frictional interface (INTER3A) elements. The fiber and matrix materials were assumed to be isotropic and linear elastic. A portion of the interface was modeled as perfectly bonded, while interface elements were used in the remaining debonded part of the interface. The interface elements could sustain only shear stress, τ_{rz}, with a magnitude less than or equal to $|\mu\sigma_{rr}|$ and compressive or zero radial stress, σ_{rr}. The formulation of the interface elements allowed separation, sliding of finite amplitude if Coulomb friction was exceeded, and arbitrary rotation of the surfaces.[17]

The finite-element mesh designed for the push-out problem is shown in Fig. A1. The mesh was considered dense enough when further refinement of any portion of the model caused less than a 0·1% change in the resulting

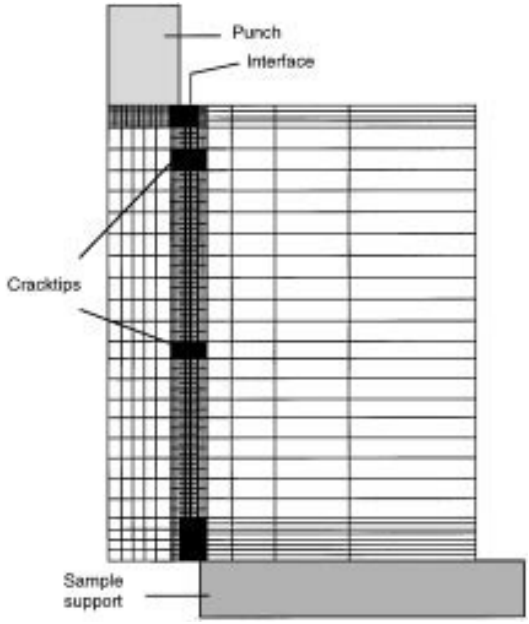

Fig. A1. Finite element mesh constructed to simulate processing and push-out loads.

total load on the top of the fiber. Although the materials were linear elastic, the solution was non-linear owing to contact being lost across part of the interface as the punch load increased and to the energy lost from the non-conservative frictional shear stress generated by the debonded portion of the fiber sliding with respect to the matrix.

Within each simulation, the push-out problem was solved in two steps. The differential thermal shrinkage load was applied in step one, and the mechanical load on the fiber top face plus the residual stress was applied in step two. The axial displacement at the bottom of the matrix was constrained in step one at $r = r_s$ to avoid rigid body motion, while nodes beyond $r = r_s$ were allowed to displace in the radial ($[u_r^m]^1(r, 0)$) and axial ($[u_z^m]^1(r, 0)$) directions. Within each step, the load was applied in increments. The entire load was applied in the first solution attempt. If the solution of the field equations was not converging quickly enough according to criteria placed on whether the field equations were satisfied (peak force residual $< 0{\cdot}005$ N) and the largest correction to a nodal variable (largest change in incremental displacement $< 0{\cdot}01\,\mu$m), the load was applied in smaller increments.

Within each increment the code solved the governing elasticity equations iteratively using a modified Newton's method. If, at the end of an iteration, one or more of the constraints in any of the interface elements was violated, the interface element(s) in question was(were) allowed to open or slip, and a new iteration was started. Typically, from 1 to 16 increments per step and less than 10 iterations per increment were necessary, depending on the debond length. The accuracy of the solution was investigated by checking whether the continuity conditions at the interface and the boundary conditions were satisfied in the same manner as described by Bechel and Sottos.[7]

APPENDIX B APPARATUS FOR FIBER PUSH-OUT TESTS AND FIBER EXTENSION TESTS

The micromechanical tester (Fig. B1) consisted of a Compumotor SX stepper motor and Daedal MS23 railtable. Displacement at the steel punch tip was measured by recording the commanded rotation of the stepper motor armature as a function of time and then subtracting machine compliance. The punch velocity was maintained at $5\,\mu\text{m}\,\text{s}^{-1}$. Load was measured by sampling a Kistler piezoelectric charge transducer at $5\,\text{sample}\,\text{s}^{-1}$. The load cell signal was conditioned by a Kistler dual mode amplifier and digitized by a Tektonix TDS 420 oscilloscope.

The testing apparatus was positioned such that the push-out/fiber extension sample was entirely illuminated by a circular polariscope. The polariscope was constructed using an argon laser (Lexel model 3500) as the light source. Since coherent light can create interference fringes, a spinning ground-glass disk was used as a coherency scrambler. A collimated beam of light passed through a polarizer which vertically polarized the light, and then through a quarter-wave plate with its fast axis at 45° to the axis of the polarizer, producing circularly polarized light. The beam continued on through the specimen, traversed a second quarter wave plate 90° out of phase with the first and through a second polarizer, eliminating the isoclinic fringes from the resulting image. Field lenses were inserted into the beam before and after the sample. The first field lens expanded the diameter of the beam from 2·5 mm to 25 mm, permitting a larger field of view, and the second field lens focused the beam on the aperture of a CCD camera (Panasonic BL200).

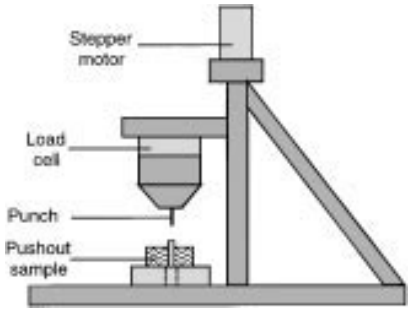

Fig. B1. Schematic of micromechanical fiber push-out tester.